



ELSEVIER

Contents lists available at ScienceDirect

Wear

journal homepage: www.elsevier.com/locate/wear

A patterned microtexture to reduce friction and increase longevity of prosthetic hip joints



Anthony Chyr^a, Mingfeng Qiu^a, Jared W. Speltz^b, Ronald L. Jacobsen^b,
Anthony P. Sanders^{a,c}, Bart Raeymaekers^{a,*}

^a Department of Mechanical Engineering, University of Utah, Salt Lake City, UT 84112, USA

^b Mound Laser & Photonics Center, Inc, Kettering, OH 45420, USA

^c Ortho Development Corp., Draper, UT 84020, USA

ARTICLE INFO

Article history:

Received 31 December 2013

Received in revised form

30 March 2014

Accepted 2 April 2014

Available online 13 April 2014

Keywords:

Prosthetic hip joint

Friction

Polyethylene

Microtexture

Laser surface texturing

ABSTRACT

More than 285,000 total hip replacement surgeries are performed in the US each year. Most prosthetic hip joints consist of a cobalt–chromium (CoCr) femoral head that articulates with a polyethylene acetabular component, lubricated with synovial fluid. The statistical survivorship of these metal-on-polyethylene prosthetic hip joints declines significantly after 10–15 years of use, primarily as a result of polyethylene wear and wear debris incited disease. The current engineering paradigm to increase the longevity of prosthetic hip joints is to improve the mechanical properties of the polyethylene component, and to manufacture ultra-smooth articulating surfaces. In contrast, we show that adding a patterned microtexture to the ultra-smooth CoCr femoral head reduces friction when articulating with the polyethylene acetabular liner. The microtexture increases the load-carrying capacity and the thickness of the joint lubricant film, which reduces contact between the articulating surfaces. As a result, friction and wear is reduced. We have used a lubrication model to design the geometry of the patterned microtexture, and experimentally demonstrate reduced friction for the microtextured compared to conventional smooth surrogate prosthetic hip joints.

© 2014 Elsevier B.V. All rights reserved.

1. Introduction

More than 285,000 total hip replacement (THR) surgeries are performed in the US each year to treat degenerative joint diseases that cause pain and disability [1]. Several bearing types for prosthetic hip joints exist: ceramic-on-ceramic (COC), ceramic-on-metal, ceramic-on-polyethylene (COP), metal-on-metal (MOM), and metal-on-polyethylene (MOP). This paper focuses on the MOP type because it is the most commonly used in the US. An MOP prosthetic hip joint consists of a femoral head, usually made of cobalt–chromium (CoCr), attached to the femur with a taper or stem. The head articulates with a polyethylene liner (usually ultra-high molecular weight polyethylene (UHMWPE) or (highly) cross-linked polyethylene (XL polyethylene)) fixed in an acetabular component that is anchored in the pelvis (see Fig. 1). The most common reasons for an MOP prosthetic hip joint to fail include [2]; (1) wear of the polyethylene liner as a result of articulation with the CoCr femoral component. Particles generated by adhesive

wear, corrosive wear, and/or abrasive wear may act as abrasives and accelerate deterioration of the sliding interface [3,4]. (2) Adverse biological reaction to indigestible microscopic wear debris leads to periprosthetic osteolysis [5–7], which undermines the implant and causes mechanical loosening and instability. Even XL polyethylene, while reducing wear [8–11], has been observed to cause osteolysis [12]. Failure of a prosthetic hip joint may lead to a risky revision surgery [13,14]. Hence, it is important to reduce friction and wear of the articulating surfaces to increase the longevity of prosthetic hip joints.

The current engineering paradigm for combating implant wear is to improve the mechanical properties of the polyethylene component and to manufacture ultra-smooth bearing surfaces, as witnessed by the re-introduction of MOM [15] and the development of COP [16] and COP prosthetic hip joints [17]. For example, COC articulating surfaces are polished to an average surface roughness $R_a < 5$ nm, which enables them to operate in the (elasto)hydrodynamic lubrication regime, thus reducing friction and wear. Despite this advantage, COC prosthetic hip joints are prone to edge-loading wear that leads to squeaking, problems that MOP hips do not exhibit. To date, the potential of reducing friction and wear by increasing the load-carrying capacity of the

* Corresponding author. Tel.: +1 801 585 7594; fax: +1 801 585 9826.

E-mail address: bart.raeymaekers@utah.edu (B. Raeymaekers).

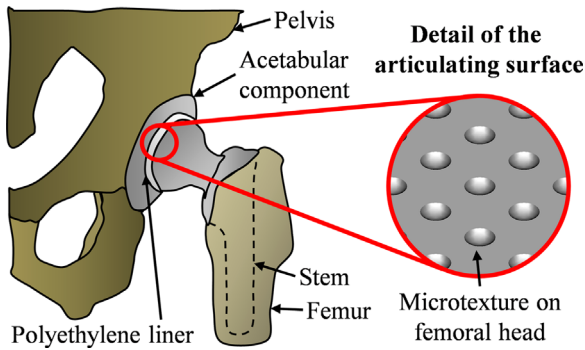


Fig. 1. Metal-on-polyethylene (MOP) prosthetic hip joint with a patterned microtexture on the CoCr femoral head.

lubricant film in MOP hips has been neglected, likely because the polymer bearing surface is compliant, prone to dimensional error, and not feasible to polish. In contrast to the existing knowledge, we attempt to decrease friction in MOP hip joints by adding a patterned microtexture to the ultra-smooth CoCr femoral head. The microtexture is implemented as an array of concave features (“dimples”) and is well-known to increase the load-carrying capacity and lubricant film thickness in other man-made bearings [18], such as, for instance, magnetic tape drives [19,20], piston rings [21], and thrust bearings [22]. The dimples form an array of microhydrodynamic bearings that increase the load-carrying capacity of the lubricant film between two bearing surfaces in relative motion. This increases the lubricant film thickness and reduces contact, thereby reducing friction and potentially wear of the articulating surfaces.

A few researchers have experimentally attempted to improve the durability of MOP prosthetic hip joints by using surface texture or increasing the surface roughness of the femoral head. Ito et al. [23] manufactured circular dimples of 0.5 mm in diameter and 0.1 mm deep, with a 1.2 mm pitch on a CoCr femoral head. They observed a 17% friction reduction and a 36% reduction in polyethylene wear, and hypothesized that this may be the result of the abrasive wear particles being trapped in the dimples and lubricant being accumulated and subsequently dispensed from the dimples during lubricant starvation conditions. Sawano et al. [24] used a waterjet to machine 0.25 μm to 4.4 μm deep channels, spaced 10 μm apart and running perpendicular to the direction of articulation, into a CoCrMo plate. A modest reduction in polyethylene wear was measured in a pin-on-disc experiment, which was attributed to the channels trapping wear particles. Zhou et al. [25] used a diamond indenter to manufacture spherical dimples of 1 mm in diameter and 2 μm deep into stainless steel plates. They conducted a pin-on-disc experiment with a UHMWPE pin (GUR 1020) and the textured stainless steel plates, and concluded that microtexture does not improve lubrication, but instead increases the surface roughness and subsequently wear. However, tall ridges were observed around the contour of the microtexture features, which may have increased friction in the bearing.

This work aims to improve the longevity of prosthetic hip joints by adding a well-defined patterned microtexture to the smooth femoral head, as illustrated in Fig. 1. The approach is opposite to the current engineering paradigm of improving prosthetic hip joint longevity by improving the mechanical properties of the polyethylene to increase wear resistance, and by manufacturing smoother articulating surfaces. It is also different from earlier research that attempted to improve longevity by using texture as lubricant reservoirs or wear particle traps.

We experimentally demonstrate reduced friction between the articulating surfaces of a textured surrogate prosthetic hip compared to a smooth one, using the exact same material pair and

surface properties of commercial prosthetic hip joints. We have used a simplified steady-state lubrication model to design the patterned microtexture geometry in terms of maximum bearing load-carrying capacity. From these results, we have selected four microtexture designs that are manufactured on convex CoCr specimens. We find that the friction coefficient between a convex CoCr specimen articulating with a concave UHMWPE specimen is reduced significantly by adding a patterned microtexture to the CoCr specimen.

2. Patterned microtexture design

2.1. Model

We use a simple steady-state lubrication model, shown in Fig. 2, to design the geometry of the patterned microtexture, in support of the experiments described in Section 3. The microtextured femoral head is represented by a column of $N=7$ dimples and moves relative to the smooth acetabular liner. Since the curvatures of the femoral head and acetabular liner are almost identical, and much larger than the dimensions of the dimple, the bearing can be approximated as a parallel slider bearing.

The following assumptions are made: (1) each dimple has an identical spherical shape and is positioned in the center of a square unit cell of width $2r_1$ (see Fig. 2(b)). (2) While it is well-known that synovial fluid is shear-thinning, its shear rate dependence is much smaller in prosthetic joints than in natural joints [26]. Hence, we model synovial fluid as a Newtonian fluid with viscosity of water at room temperature [27,28], which is a conservative assumption. The viscosity of synovial fluid (and bovine serum) is typically larger, which would increase the hydrodynamic pressure in our model. (3) Inertial forces are neglected because they are at least two orders of magnitude smaller than the viscous forces. (4) The minimum spacing c between the bearing surfaces is sufficient to avoid asperity contact and, thus, hydrodynamic lubrication is maintained assuming abundant lubricant supply. (5) No slip is assumed at the solid boundaries. Thus, the relationship between bearing spacing and pressure is governed by the steady-state two-dimensional incompressible Reynolds equation, given in dimensional form as [29]

$$\frac{\partial}{\partial x} \left(h^3 \frac{\partial p}{\partial x} \right) + \frac{\partial}{\partial y} \left(h^3 \frac{\partial p}{\partial y} \right) = 6\mu U \frac{\partial h}{\partial x} \quad (1)$$

where x and y are Cartesian coordinates as indicated in Fig. 2, $p(x,y)$ is the local bearing pressure, $h(x,y)$ is the local bearing spacing, μ is the dynamic viscosity of the lubricant, and U is the relative sliding

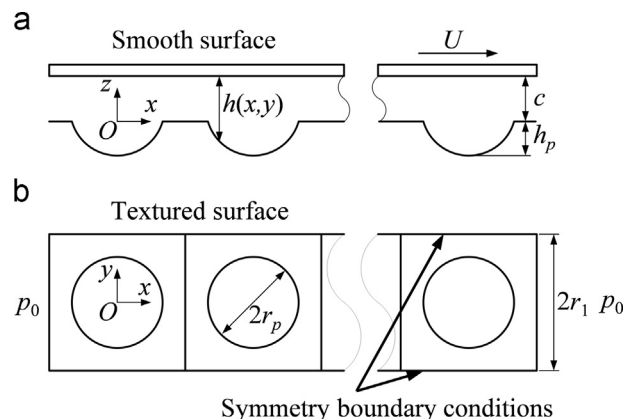


Fig. 2. Schematic of the lubrication model showing (a) cross-sectional view and (b) top view.

velocity between the microtextured and smooth surfaces. Eq. (1) can be rewritten in non-dimensional form as

$$\frac{\partial}{\partial X} \left(H^3 \frac{\partial P}{\partial X} \right) + \frac{\partial}{\partial Y} \left(H^3 \frac{\partial P}{\partial Y} \right) = \frac{\lambda}{\delta^2} \frac{\partial H}{\partial X}, \quad (2)$$

where $X=x/r_p$, $Y=y/r_p$, $P(X,Y)=p(x,y)/p_0$, $H(X,Y)=h(x,y)/c$. r_p denotes the dimple radius and c is the minimum bearing spacing. The non-dimensional flow factor $\lambda=3\mu U/(2r_p p_0)$ and the non-dimensional minimum spacing $\delta=c/(2r_p)$ define the operating conditions of the bearing. The inlet and outlet of the column of N dimples are maintained at ambient pressure p_0 . Symmetric boundary conditions are used on the lateral edges, to mimic the presence of adjacent dimples. Thus,

$$P\left(-\frac{r_1}{r_p}, Y\right) = P\left(\left(N-\frac{1}{2}\right)\frac{2r_1}{r_p}, Y\right) = 1, \quad (3a)$$

$$\frac{\partial P}{\partial Y}\left(X, -\frac{r_1}{r_p}\right) = \frac{\partial P}{\partial Y}\left(X, \frac{r_1}{r_p}\right) = 0, \quad (3b)$$

with respect to the origin of the coordinate system shown in Fig. 2. Reynolds cavitation is implemented to account for gaseous cavitation in the lubricant [29], and the cavitation pressure is assumed to be 90% of ambient pressure. This is similar to what others have used to describe gaseous cavitation in traditional smooth prosthetic hip joints [30]. The patterned microtexture is uniquely described by its texture aspect ratio, $\varepsilon=h_p/(2r_p)$, and texture density, $S_p=\pi r_p^2/(4r_1^2)$. In each dimple cell, the non-dimensional local spacing $H(X,Y)$ between the smooth and microtextured surface with spherical dimples is given with respect to a local coordinate system with the origin coincident with the center of the cell as

$$H(X,Y) = \begin{cases} 1, & \text{if } X^2 + Y^2 > 1 \\ 1 + \frac{1}{2\delta} \sqrt{\left(\varepsilon + \frac{1}{4\varepsilon}\right)^2 - (X^2 + Y^2)} - \frac{1}{2\delta} \left(\frac{1}{4\varepsilon} - \varepsilon\right), & \text{if } X^2 + Y^2 \leq 1 \end{cases} \quad (4)$$

2.2. Simulation results

We have used a finite difference approach on a staggered grid [31,32] with a successive over-relaxation factor of 1.0–1.9 to solve Eqs. (2) and (3) in conjunction with the Reynolds cavitation condition, for a range of different microtexture geometries (ε , S_p). The operating conditions $\lambda=5.94 \times 10^{-4}$ and $\delta=0.01$ are maintained constant, because the optimal microtexture geometry is almost independent of the operating conditions [33]. Convergence of the numerical solution is obtained when the relative change between two successive iterations of the pressure solution is smaller than 10^{-6} at each grid point. A uniform grid of 301 by 301 nodes per unit cell is selected based on mesh convergence analysis, and further refining the grid does not change the solution by more than 2%. Fig. 3 shows the non-dimensional load-carrying capacity per unit area, $W=(P_{avg}-1)$, as a function of texture density and texture aspect ratio. $P_{avg}=p_{avg}/p_0$ is the average non-dimensional bearing pressure. Four different microtexture designs (ε , S_p) are identified in Fig. 3.

3. Friction experiments

3.1. Experimental apparatus

We experimentally demonstrate that adding a patterned microtexture to the ultra-smooth CoCr surface reduces the friction coefficient between the articulating surfaces of the surrogate prosthetic hip bearing. Fig. 4 shows a schematic of the friction experiment. We use a CoCr cylinder as surrogate femoral head and

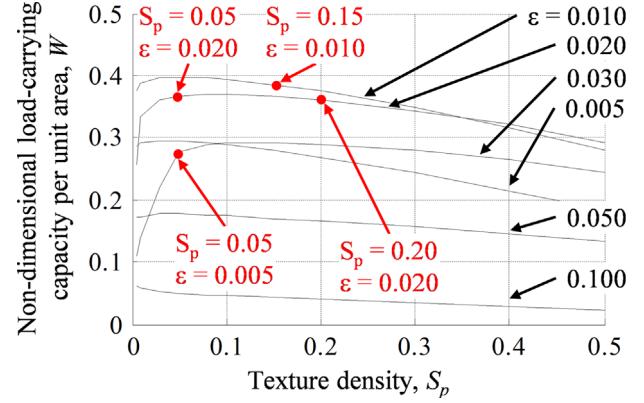


Fig. 3. Non-dimensional load-carrying capacity per unit area as a function of texture density and texture aspect ratio for $\lambda=5.94 \times 10^{-4}$ and $\delta=0.01$. The results show that an optimal combination of ε and S_p exists that maximizes the load-carrying capacity or, correspondingly, maximizes the lubricant film thickness. Four patterned microtexture designs are selected and manufactured on surrogate CoCr femoral heads.

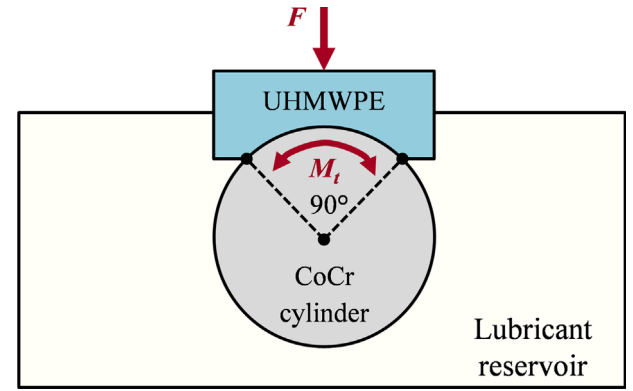


Fig. 4. Schematic of the friction experiment.

a concave cylindrical UHMWPE specimen as surrogate acetabular liner. The CoCr cylinder rotates reciprocally according to a prescribed kinematic cycle over a span of $\theta=90^\circ$, while pressed against the concave UHMWPE specimen with load F . This simulates the flexion/extension rotation and axial loading of the prosthetic hip joint, which are the primary kinematic and loading components, respectively. The friction coefficient is computed from torque M_t and normal load F measurements, for both a microtextured and smooth CoCr cylinder, articulating with a smooth UHMWPE specimen. The bearing surfaces are submerged in bovine serum (HyClone – 20 mg/ml protein concentration).

Fig. 5(a) depicts the experimental apparatus, adapted from a knee tester of which the design, instrumentation and operating details are discussed elsewhere [34]. The setup consists of a reciprocating rotating shaft supported in two flange bearings (Fig. 5(b)), driven by a geared stepper motor. The CoCr specimen is mounted on the shaft, and the concave UHMWPE specimen is loaded against the CoCr specimen using compression springs and a power screw mechanism. The magnitude of the load F is controlled using a force feedback control system. A torque sensor and load cell measure M_t and F between the articulating cylindrical CoCr and UHMWPE specimens, respectively (Fig. 5(c)), see also Section 3.2), from which the friction coefficient as a function of time is determined. A reservoir contains bovine serum lubricant, submerging the interface between the articulating surfaces.

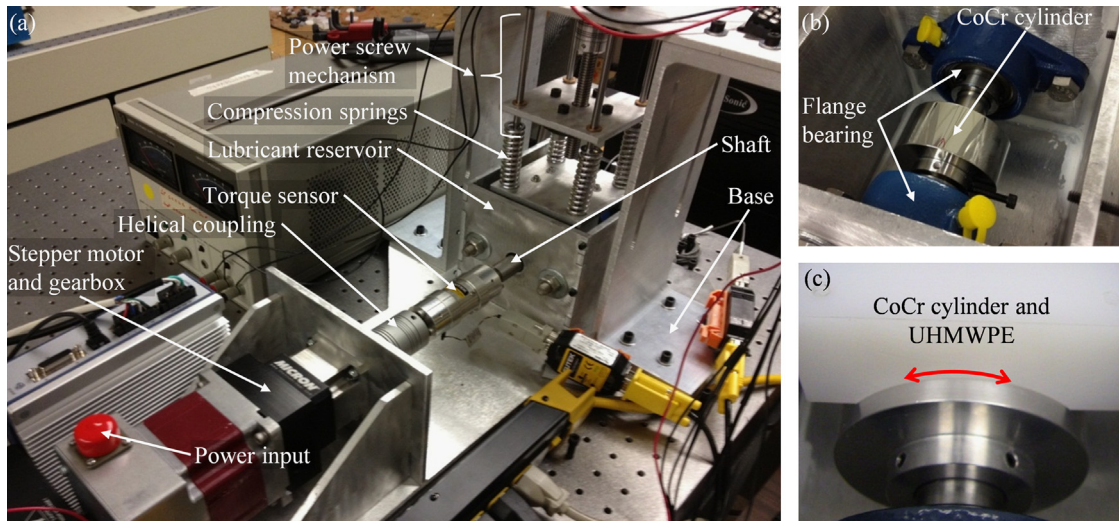


Fig. 5. Experimental apparatus (a) overview picture, (b) detail of the cylindrical CoCr cylinder mounted on the reciprocating shaft in the reservoir, and (c) detail of the interacting CoCr and UHMWPE articulating surfaces [34].

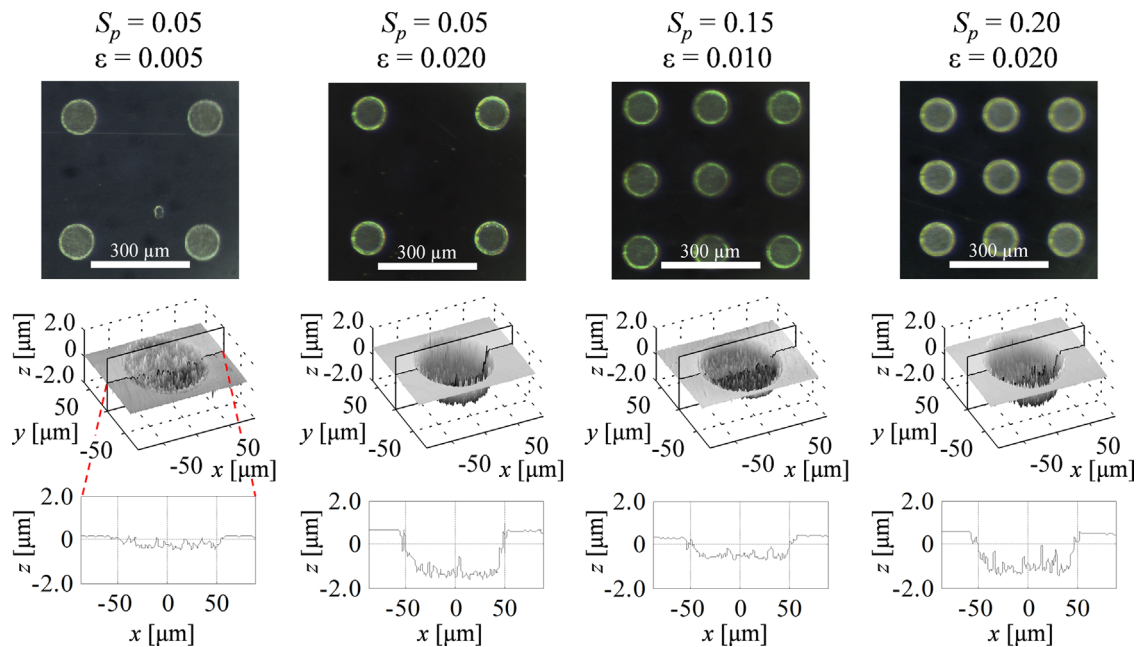


Fig. 6. Optical microscope and white light interferometer images of each of the four patterned microtexture designs, manufactured on cylindrical CoCr specimens (ASTM F1537-08), showing the results of the LST process. A trace along the centerline of the dimple reveals the surface roughness inside the dimple. The radius of the dimples, $r_p = 50 \mu\text{m}$.

3.2. Specimens

We have used laser surface texturing (LST) with a solid-state laser to manufacture the patterned microtexture designs on smooth, CoCr (ASTM F1537-08) cylinders with a diameter of 50 mm, polished to $R_a < 50 \text{ nm}$. The dimple radius $r_p = 50 \mu\text{m}$, for the four microtexture designs. Fig. 6 shows optical microscopy and white light interferometry images of each of the four microtexture patterns on the CoCr cylinders. A cross-section through the center line of the dimple reveals the surface roughness inside the dimples. Minimal material deposition around the contour of each dimple, resulting from the LST process, is observed. Fig. 7(a) and (b) shows a photograph and a white light interferometry image, respectively, of a smooth cylindrical CoCr specimen, used as benchmark in the friction experiments. Additionally, Fig. 8 depicts the concave UHMWPE (GUR 1020-ASTM F648) specimen of

diameter 50.75 mm, and machined to $R_a = 500 \text{ nm}$. Both the CoCr and UHMWPE specimens are manufactured and finished to identical specifications as commercial MOP prosthetic hip joints. The conformity ratio between the articulating surfaces is 98.5%. The contact pressure (0.57–1.13 MPa) is calculated using the Hertz theory and falls within the range of in-vivo values [35,36].

3.3. Methods

Fig. 9 illustrates the experimental methodology. Fig. 9(a) shows the kinematic cycle including velocity and angular position of the CoCr cylinder with respect to the concave UHMWPE counterface as a function of time. The kinematic cycle is designed to maximize the portion during which a constant sliding velocity is maintained, to best approach the steady-state lubrication model used to optimize the microtexture geometry. The frequency of the kinematic cycle is

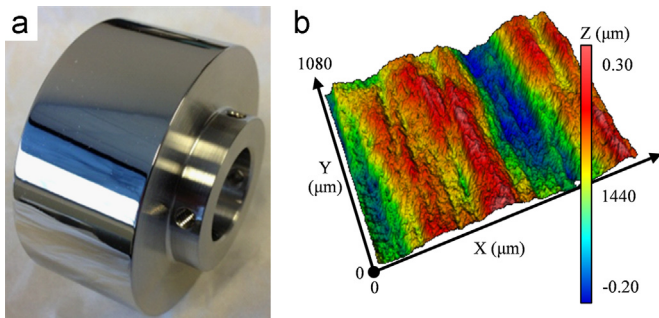


Fig. 7. Smooth cylindrical CoCr specimen (a) photograph and (b) white light interferometer image of the articulating surface.

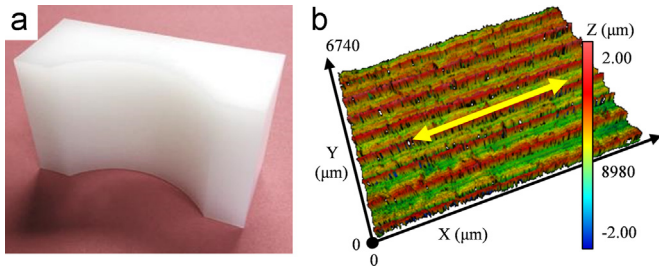


Fig. 8. UHMWPE specimen (a) photograph and (b) white light interferometer image of the articulating surface. The yellow arrow indicates the direction of articulation. (For interpretation of the references to color in this figure legend, the reader is referred to the web version of this article.)

1.0 Hz [37] (ISO 14242-1), similar to walking gait. Fig. 9(b) shows the friction coefficient f as a function of time for the textured ($S_p=0.05$, $\epsilon=0.005$) and smooth CoCr cylinders, respectively, articulating against the UHMWPE specimen. Only two seconds of data are shown, extracted from a long-duration experiment, to illustrate the detailed measurement of the friction coefficient as a function of time. The maximum contact pressure between the CoCr cylinder and the UHMWPE specimen in this example experiment is 0.71 MPa.

4. Results and discussion

From Fig. 9(b) we observe that the friction coefficient is periodic with reversals between clockwise (CW) and counter-clockwise (CCW) rotations. The friction coefficient is maximum at start and stop ($t=0.5, 1.0, 1.5$ s), and minimum in the middle of each cycle, when the sliding velocity at the surface of the cylinder is constant (0.1 m/s). The microtextured CoCr specimen outperforms the smooth specimen in two ways. First, the friction coefficient is significantly lower for the microtextured compared to the smooth cylinder over almost the entire kinematic cycle (for this particular microtexture geometry and kinematic cycle example). However, the measured values of the friction coefficient (approximately $f=0.15$ – 0.20), do not seem to indicate full fluid lubrication. Rather, this indicates reduced contact between the microtextured CoCr and UHMWPE surfaces, as a result of the increased bearing load-carrying capacity generated by the patterned microtexture. Second, the friction coefficient in the case of the microtextured CoCr cylinder decreases much faster immediately after reversing the sliding direction, compared to the smooth CoCr cylinder. This is indicated by the sharp drop of the friction coefficient surrounding direction reversals (at $t=0.5, 1.0, 1.5$ s). The increased load-carrying capacity generated by the patterned microtexture increases the portion of the bearing load that is carried by the lubricant faster than in the case of a smooth surface. This reduces asperity contact and friction between the articulating surfaces.

Table 1 shows the average friction coefficient calculated over a single 1 Hz cycle extracted from a long duration experiment, for all four patterned microtexture designs articulating with a UHMWPE specimen, and for different values of the contact pressure, ranging between 0.57–1.13 MPa. The kinematic cycle is identical to the one shown in Fig. 9(a) and the specimens are fully submerged in bovine serum. From Table 1 we observe that the average friction coefficient increases with increasing contact pressure, for both smooth and microtextured CoCr cylinders. In all cases, the smooth specimen never outperforms the microtextured ones, except for the cases with contact pressure of 1.13 MPa. The increased load-carrying capacity generated by the patterned microtexture is not sufficient to reduce contact between the articulating bearing surfaces. Thus, solid-on-solid contact occurs between the microtextured CoCr and UHMWPE specimens, which results in a higher friction coefficient than the contact between the smooth CoCr and UHMWPE specimens.

We have also quantified the portion of the kinematic cycle during which each of the microtextured CoCr specimens displays a lower friction coefficient than the smooth CoCr specimen, to evaluate and compare the performance of the four patterned microtexture designs. Table 2 summarizes the results and shows the percentage of the kinematic cycle during which the microtextured CoCr cylinder outperforms the smooth one. From Table 2 we observe that each microtexture design outperforms the traditional smooth surface over at least part of the kinematic cycle. However, the portion during which the microtextured CoCr cylinder outperforms the smooth one decreases with increasing contact pressure. This is similar to the results shown in Table 1. With increasing contact pressure, the patterned microtexture does not generate enough hydrodynamic pressure to support the increased bearing load and reduce friction between the articulating surfaces.

These results support the hypothesis that friction can be reduced at low sliding velocities in a surrogate MOP prosthetic hip joint by means of a patterned microtexture on the surface of

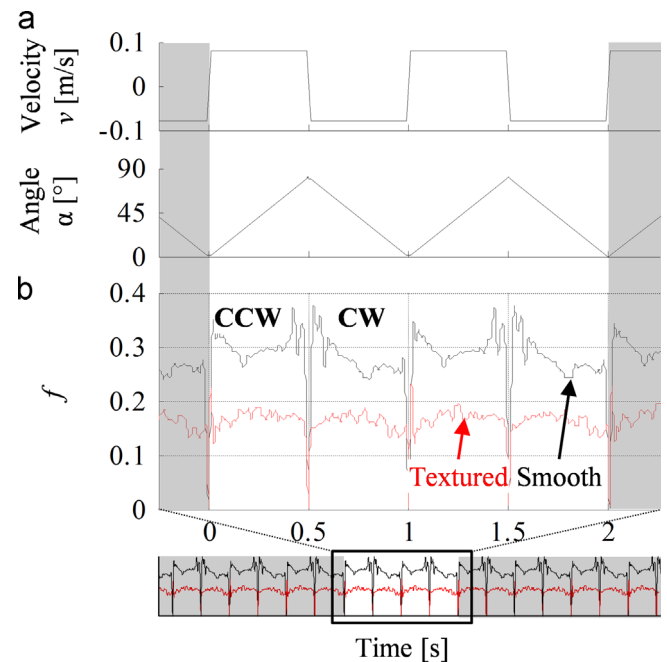


Fig. 9. (a) Kinematic cycle of the CoCr specimen articulating with the UHMWPE specimen. (b) Friction coefficient as a function of time for the microtextured (red) specimen ($S_p=0.05$, $\epsilon=0.005$) and the smooth (black) specimen, showing that the microtextured specimen outperforms the smooth specimen over almost the entire kinematic cycle. (For interpretation of the references to color in this figure legend, the reader is referred to the web version of this article.)

the femoral head. However, at very high contact pressures the hydrodynamic pressure generated by the patterned microtexture may not be large enough to support the bearing load. As a result, contact occurs between the articulating surfaces, and the microtextured CoCr specimen may underperform the smooth one.

The relative performance of the different microtexture designs does not correlate well with the predicted load-carrying capacity (Fig. 3). Several reasons contribute to this observation. First, we find that the manufacturing tolerance of shallow dimples is not held accurately while texturing the entire CoCr specimen. The error of the depth of the dimple may be as high as 50% for the microtexture design with $\epsilon=0.005$ but decreases with increasing ϵ . Second, the relative differences in the load-carrying capacity predicted by the model for the four different microtexture designs is small. Thus, minor misalignment of the experimental apparatus, or other external parameters could account for the difference between the experimental and theoretical results. Also, the assumption of full fluid lubrication is likely not satisfied in the experiments as the friction coefficient values seem to indicate mixed lubrication rather than full fluid lubrication. The lubrication model could also be improved by including elastic deformation of the UHMWPE specimen, i.e., using an elastohydrodynamic lubrication (EHL) model instead of a hydrodynamic lubrication model. However, using EHL with a fine numerical grid, needed to resolve the pressure gradients in the dimples, is computationally expensive. However, since the objective of this work is to experimentally demonstrate the concept of microtexture in prosthetic hip joints, the model is only used to guide the choice of texture geometries.

A limitation of the experiments is side-leakage between the articulating cylindrical specimens compared to a ball-in-socket hip prosthesis. Side-leakage is minimal, however, because the unidirectional motion is orthogonal to the sides of the bearing where leakage occurs. Additionally, it is well known that the boundary effects in textured bearings are limited to the first few rows of dimples adjacent to the boundary. Furthermore, a prosthetic hip joint experiences six degrees of freedom. The most important kinematic component during gait is the flexion/extension (FE) rotation, although other motions create cross-shear in the polyethylene, which markedly affects wear. The experimental apparatus only simulates single-direction FE motion, which limits its scope to investigating the effect of reducing friction. Friction can be an

Table 1
Average kinematic friction coefficient for different microtexture designs and contact pressures.

Texture design 	Texture parameters S_p, ϵ	Max contact pressure [MPa]			
		0.57	0.71	0.90	1.13
	Smooth	0.26	0.29	0.29	0.28
	$S_p=0.05,$ $\epsilon=0.005$	0.12	0.17	0.23	0.29
	$S_p=0.05,$ $\epsilon=0.020$	0.20	0.26	0.28	0.31
	$S_p=0.15,$ $\epsilon=0.010$	0.19	0.21	0.25	0.29
	$S_p=0.20,$ $\epsilon=0.020$	0.16	0.24	0.25	0.29

Table 2

Different microtexture designs, showing the percentage of the 1 Hz kinematic cycle during which the microtextured CoCr specimen outperforms the smooth CoCr specimen, for different values of constant bearing contact pressure.

Texture design 	Texture parameters S_p, ϵ	Max contact pressure [MPa]			
		0.57	0.71	0.90	1.13
	$S_p=0.05,$ $\epsilon=0.005$	98%	98%	94%	24%
	$S_p=0.05,$ $\epsilon=0.020$	88%	67%	58%	19%
	$S_p=0.15,$ $\epsilon=0.010$	94%	96%	91%	22%
	$S_p=0.20,$ $\epsilon=0.020$	93%	90%	83%	15%

important predictor of wear, and by reducing friction, we indicate the potential of reducing wear in future hip simulator tests that take all degrees of freedom of the prosthetic hip into account.

5. Conclusion

Based on our numerical and experimental results, we find that the friction coefficient between the surrogate convex CoCr and the concave UHMWPE specimens is lower for a microtextured CoCr specimen, than for the benchmark smooth CoCr specimen. The results demonstrate that the patterned microtexture reduces friction by increasing the hydrodynamic pressure and thickness of the lubricant film. This is observed for the four microtexture designs and all values of the contact pressure considered in this study, with the exception of the highest contact pressure we have used. In that case, the increased load-carrying capacity generated by the microtexture is not sufficient to support the bearing load and reduce friction.

The inherent limitations of the simple model that we used undoubtedly affect the correlation with the experimental results. Elastic deformation of the polyethylene is not accounted for, and a more sophisticated elastohydrodynamic lubrication model would likely be more accurate. However, the simple model-based design of the microtexture geometry is fast and allows obtaining a range of microtexture parameters that are suitable to reduce friction in the prosthetic hip joint. A reduced friction coefficient between the articulating bearing surfaces promises reduced wear and increased longevity of the prosthetic hip joint. Also, in contrast with the smooth surrogate CoCr femoral head, the friction coefficient decreases very quickly after reversal of the sliding direction for the microtextured surrogate femoral heads. Daily human joint activity includes frequent starts and stops, and it is during these periods of high friction that the most wear occurs. Thus, the microtexture reduces friction and potentially wear precisely where it is most needed.

Acknowledgments

This work was partially funded through NSF award #1227869, NIH award #1R41AR064095-01 and a University of Utah Technology Commercialization grant. Anthony Chyr also acknowledges partial funding through an Undergraduate Research Opportunity (UROP) award from the University of Utah, and through the

Society of Tribologists and Lubrication Engineers (STLE) E.R. Booser Presidential Award.

References

- [1] American Academy of Orthopaedic Surgeons, Total Hip Replacement. Available from: (<http://orthoinfo.aaos.org/topic.cfm?topic=A00377>).
- [2] K.J. Bozic, S.M. Kurtz, E. Lau, K. Ong, T.P. Vail, D.J. Berry, The epidemiology of revision total hip arthroplasty in the united states, *J. Bone Jt. Surg. Am.* 91 (2009) 128–133.
- [3] A. Wang, A. Essner, V.K. Polineni, C. Stark, J.H. Dumbleton, Lubrication and wear of ultra-high molecular weight polyethylene in total joint replacements, *Tribol. Int.* 31 (1–3) (1998) 17–33.
- [4] J. Fisher, Wear of ultra-high molecular weight polyethylene in total artificial joints, *Curr. Orthop.* 8 (3) (1994) 164.
- [5] W.H. Harris, Wear and periprosthetic osteolysis: the problem, *Clin. Orthop. Relat. Res.* (2001) 66–70 (393).
- [6] A. Marshall, M.D. Ries, W. Paprosky, How prevalent are implant wear and osteolysis, and how has the scope of osteolysis changed since 2000? *J. Am. Acad. Orthop. Surg.* 16 (Suppl 1) (2008) S1–S6.
- [7] E. Garcia-Rey, E. Garcia-Cimbrelo, A. Cruz, J. Ortega-Chamarro, New types of polyethylene in total hip replacement: prospective and comparative clinical study on wear, *J. Bone Jt. Surg. Br.* 91-B (Suppl. II) (2009) S318.
- [8] H. McKellop, F.W. Shen, B. Lu, P. Campbell, R. Salovey, Development of an extremely wear-resistant ultra high molecular weight polyethylene for total hip replacements, *J. Orthop. Res.* 17 (2) (1999) 157–167.
- [9] H. McKellop, F.W. Shen, B. Lu, P. Campbell, R. Salovey, Effect of sterilization method and other modifications on the wear resistance of acetabular cups made of ultra-high molecular weight polyethylene. A hip-simulator study, *J. Bone Jt. Surg. Am.* 81-A (12) (2000) 1708–1725.
- [10] O.K. Muratoglu, C.R. Bragdon, D.O. O'Connor, M. Jasty, W.H. Harris, A novel method of cross-linking ultra-high-molecular-weight polyethylene to improve wear, reduce oxidation, and retain mechanical properties, *J. Arthroplasty* 16 (2) (2001) 149–160.
- [11] C. Heisel, M. Silva, M.A. dela Rosa, T.P. Schmalzried, Short-term in vivo wear of cross-linked polyethylene, *J. Bone Jt. Surg. Am.* 86-A (4) (2004) 748–751.
- [12] L. Bradford, R. Kurland, M. Sankaran, H. Kim, L.A. Pruitt, M.D. Ries, Early failure due to osteolysis associated with contemporary highly cross-linked ultra-high molecular weight polyethylene. A case report, *J. Bone Jt. Surg. Am.* 86-A (5) (2004) 1051–1056.
- [13] S. Kurtz, F. Mowat, K. Ong, N. Chan, E. Lau, M. Halpern, Prevalence of primary and revision total hip and knee arthroplasty in the United States from 1990 through 2002, *J. Bone Jt. Surg. Am.* 87 (7) (2005) 1487–1497.
- [14] K. Ong, E. Lau, J. Suggs, S. Kurtz, M. Manley, Risk of subsequent revision after primary and revision total joint arthroplasty, *Clin. Orthop. Rel. Res.* 468 (11) (2010) 3070–3076.
- [15] D. Dowson, Z.M. Jin, Metal-on-metal hip joint tribology, *Proc. Inst. Mech. Eng. Part H* 220 (2) (2006) 107–118.
- [16] C.J. Sychterz, C.A. Engh Jr., A.M. Young, R.H. Hopper Jr., C.A. Engh, Comparison of in vivo wear between polyethylene liners articulating with ceramic and cobalt-chrome femoral heads, *J. Bone Jt. Surg. B* 82 (7) (2000) 948–951.
- [17] M.N. Rahaman, A. Yao, B.S. Bal, J.P. Garino, M.D. Ries, Ceramics for prosthetic hip and knee joint replacement, *J. Am. Ceram. Soc.* 90 (7) (2007) 1965–1988.
- [18] I. Etsion, State-of-the-art in laser surface texturing, *J. Tribol. Trans. ASME* 127 (1) (2005) 248–253.
- [19] B. Raeymaekers, I. Etsion, F.E. Talke, Enhancing tribological performance of the magnetic tape/guide interface by laser surface texturing, *Tribol. Lett.* 27 (1) (2007) 89–95.
- [20] B. Raeymaekers, I. Etsion, F.E. Talke, A model for magnetic tape/guide friction reduction by laser surface texturing, *Tribol. Lett.* 28 (1) (2007) 9–17.
- [21] G. Ryk, Y. Kligerman, I. Etsion, Experimental investigation of laser surface texturing for reciprocating automotive components, *Tribol. Trans.* 45 (4) (2002) 444–449.
- [22] V. Brizmer, Y. Kligerman, I. Etsion, A laser surface textured parallel thrust bearing, *Tribol. Trans.* 46 (3) (2003) 397–403.
- [23] H. Ito, K. Kaneda, T. Yuhta, I. Nishimura, K. Yasuda, T. Matsuno, Reduction of polyethylene wear by concave dimples on the frictional surface in artificial hip joints, *J. Arthroplasty* 15 (3) (2000) 332–338.
- [24] H. Sawano, S.I. Warisawa, S. Ishihara, Study on long life of artificial joints by investigating optimal sliding surface geometry for improvement in wear resistance, *Precis. Eng.* 33 (4) (2009) 492–498.
- [25] X. Zhou, A.L. Galvin, Z. Jin, X. Yan, J. Fisher, The influence of concave dimples on the metallic counterface on the wear of ultra-high molecular weight polyethylene, *Proc. Inst. Mech. Eng. J* 226 (6) (2011) 455–462.
- [26] D. Mazzucco, G. McKinley, R.D. Scott, M. Spector, Rheology of joint fluid in total knee arthroplasty patient, *J. Orthop. Res.* 20 (2002) 1157–1163.
- [27] A. Cooke, D. Dowson, V. Wright, The rheology of synovial fluid and some potential synthetic lubricants for degenerate synovial fluid, *Eng. Med.* 7 (2) (1978) 66–72.
- [28] Z. Jin, D. Dowson, J. Fisher, Analysis of fluid film lubrication in artificial hip joint replacements with surfaces of high elastic modulus, *Proc. Inst. Mech. Eng. H* 211 (3) (1997) 247–256.
- [29] O. Pinkus, B. Sternlicht, *Theory of Hydrodynamic Lubrication*, McGraw-Hill, New York, 1961.
- [30] F.C. Wang, Z.M. Jin, Elastohydrodynamic lubrication modeling of artificial hip joints under steady-state conditions, *J. Tribol. Trans ASME* 127 (2005) 729–739.
- [31] M. Qiu, A. Delic, B. Raeymaekers, The effect of texture shape on the load-carrying capacity of gas-lubricated parallel slider bearings, *Tribol. Lett.* 48 (3) (2012) 315–327.
- [32] M. Qiu, B.R. Minson, B. Raeymaekers, The effect of texture shape on the friction coefficient and stiffness of gas lubricated parallel slider bearings, *Trib. Int.* 67 (2013) 278–288.
- [33] A. Shinkarenko, Y. Kligerman, I. Etsion, The effect of surface texturing in soft elasto-hydrodynamic lubrication, *Tribol. Int.* 42 (2) (2009) 284–292.
- [34] A. Chyr, A. Sanders, B. Raeymaekers, A hybrid apparatus for friction and accelerated wear testing of total knee replacement bearing materials, *Wear* 308 (2013) 54–60.
- [35] W.A. Hodge, R.S. Fijan, K.L. Carlson, R.G. Burgess, W.H. Harris, R.W. Mann, Contact pressures in the human hip joint measured in vivo, *Proc. Natl. Acad. Sci. USA* 83 (9) (1986) 2879–2883.
- [36] D.E. Krebs, L. Elbaum, P.O. Riley, W.A. Hodge, R.W. Mann, Exercise and gait effects on in vivo hip contact pressures, *Phys. Ther.* 71 (4) (1991) 301–309.
- [37] M.P. Murray, A.B. Drought, R.C. Kory, Walking patterns of normal men, *J. Bone Jt. Surg.* 46 (2) (1964) 335–360.